Optical properties of self-affine thin films

Vladimir M. Shalaev
Department of Physics, New Mexico State University, Las Cruces, New Mexico 88003

R. Botet
Laboratoire de Physique des Solides, Université Paris-Sud, Centre d'Orsay, 91405 Orsay Cedex, France

J. Mercer and E. B. Stechel
Sandia National Laboratories, Albuquerque, New Mexico 87185
(Received 29 January 1996; revised manuscript received 22 May 1996)

Optical properties of self-affine thin films are studied in the quasistatic approximation. The eigenmodes of a self-affine surface manifest strongly inhomogeneous spatial distributions characterized by various degree of localization. On a metal self-affine film, the intensities in areas of high local fields (''hot'' zones) exceed the applied field intensity by approximately three orders of magnitude. The spatial locations of the hot zones are very strong functions of the frequency and polarization of the incident light. [S0163-1829(96)08435-4]

It is well known that surfaces formed by condensing atomic beams onto a low temperature substrate are characterized by microscopic surface roughness.[1] A number of optical phenomena are strongly enhanced on a rough metal film.[2] This enhancement is commonly associated with excitation of surface plasmon oscillations. Two varieties of surface plasmons are typically recognized: (1) surface plasmon waves (SPW's) and localized surface plasmons (LSP's). SPW's propagate laterally along the metal surface; LSP's are confined to metal particles that are much smaller in size than the wavelength of the incident light.

Recent evidence suggests that cold-deposited metal films are self-affine fractal structures.[1,3] Self-affine surfaces obtained in the process of film growth belong to the Kardar-Parisi-Zhang universality class.[4] Unlike statistically self-similar structures, in order to reveal scale invariance, a self-affine surface (SAS) requires different scaling factors in the (x,y) plane and in the normal direction, z.

Fractal structures do not possess translational invariance, and ordinary running waves (such as SPW's) are not, in general, eigenmodes of a self-affine surface. Also, we anticipate that plasmon oscillations associated with different roughness features strongly interact with each other via dipolar or, more generally, multipolar forces. Thus, plasmon oscillations on a self-affine surface are neither conventional SPW's nor independent LSP's. They should be treated as collective eigenmodes which are formed by the interaction between different features of a self-affine film.

Contrary to the case of ''usual'' roughness, there is no correlation length for self-affine surfaces, which means that the inhomogeneities of all sizes are present according to a power-law distribution.[5] A self-affine surface is ''prickly''; in particular, it contains roughness features of very small (asymptotically zero) radii of curvature, i.e., the profile's derivatives can be very large. (Of course, this kind of divergence is only formal, because scale invariance appears as intermediate asymptotics between, at least, the atomic length scale and the size of a sample.) Unlike a random surface with small spatial inhomogeneities, the contribution of highest spatial harmonics (with the amplitude larger than the harmonic wavelength) does play an important role in the Fourier decomposition of a self-affine surface. All this means that neither the Rayleigh perturbation approximation[6–8] nor a Kirchoff (geometrical optics) approach can be applied to describe optical properties of a self-affine structure.[9] (Apart from the two basic approaches, there is in existence a phase perturbation approach,[10,11] which is in some sense intermediate between these two basic methods and also cannot be applied for a self-affine surface.)

An alternative approach is based on the microscopic ''discrete dipole approximation'' (DDA) which was suggested by Purcell and Pennypacker[12] and developed by Draine[13] for calculation of the optical response of an object of arbitrary shape. (A self-affine film can be thought of as a special kind of an odd-shaped object.) The DDA replaces the solid object by an array of N point dipoles, with the spacing between the dipoles small compared to the wavelength and sizes of spatial inhomogeneities. Each dipole has an oscillating polarization in response to both an incident wave and the electric fields due to all of the dipoles in the array; the self-consistent solution for the dipole polarizations can be obtained as the solution to a set of coupled-dipole equations (CDE's).

For the polarizability, α_0, of each individual dipole, the Clausius-Mossotti relation is used:[12–14]

$$\alpha_0 = \frac{3}{4\pi n}\,\frac{\epsilon-1}{\epsilon+2}, \tag{1}$$

where $\epsilon=\epsilon(\lambda)$ is the bulk dielectric function and n is the number density of dipoles. For polarizable point dipoles located on a cubic lattice, this relation is exact in the zero-frequency limit. (At finite frequencies, small corrections appearing due to a radiative reaction can be typically neglected.) If the lattice period is a, then the density number $n=a^{-3}$.

The known formula for the polarizability of a dielectric sphere in vacuum is given by the expression similar to (1),

$$\alpha_0 = R_m^3 \frac{\epsilon - 1}{\epsilon + 2}, \tag{2}$$

where R_m is the radius of the spherical monomer. Comparing (1) and (2), we conclude that instead of point dipoles, one can equally employ spherical particles (monomers) placed on a cubic lattice in the volume of an object. To make the formulas (1) and (2) identical, the radius of monomers, R_m, must be chosen so that

$$a^3 = (4\pi/3) R_m^3. \tag{3}$$

This relation implies that the spheres slightly overlap, so that the total volume of all the spheres is equal to the volume of the original object under consideration.

Remarkably, the solutions to the CDE, with α_0 defined in (1) or (2) and (3), accurately describe the optical response of an object within the purely dipole approximation.[12–16] In this regard, it is worth noting that the Maxwell equations in macroscopic media also contain only dipoles (via the polarization term).

To simulate a self-affine film, we use the restricted solid-on-solid (RSS) model.[17,18] In this model, a particle is incorporated into the growing aggregate only if the newly created interface does not have steps which are higher than one lattice unit, a. The surface structure of such deposits is relatively simple, because there are no overhangs. In this way strong corrections to scaling effects are eliminated and the true scaling behavior appears clearly, even for small dimensions. In the long-time regime, the height-height correlation function for a self-affine surface has the form[17,18]

$$\langle [h(\mathbf{R}) - h(0)]^2 \rangle \sim R^{2H}, \tag{4}$$

where $\mathbf{R}$ is the radius vector in the plane normal to the growth direction, z, and the scaling exponent (codimension), H, is related to the fractal dimension, D, through the formula $H = 3 - D$. For the RSS model, $D = 2.6$ and the scaling formula (4) is valid for large values of the average height, h, (which is proportional to the deposition time), such that $h \gg l^{\zeta}$, where $\zeta = 2(d+1)/(d+2) = 2 - H$ (l is the linear size of a system and d is the dimension of the embedding space).[18] Our simulations satisfied this condition, and the scaling relation (4) is well pronounced.

In the simulations, we removed the bulk (regular) part of the computer-generated film so that the resultant sample had, at least, one hole. Clearly, the removal of the bulk part of a film does not affect the scaling condition (4). A typical simulated self-affine film is shown in Fig. 1.

Below, we assume that the (lateral) size of a sample, l, is much less than the wavelength, $l \ll \lambda$, so that the quasistatic approximation is valid. (For example, for $\lambda = 1$ μm, the length, l, and the height, h, can be in the range from 0.1 to 0.5 μm and 10 nm to 100 nm, respectively.) Then, the coupled-dipole equations have the form[12,16]

$$d_{i,\alpha} = \alpha_0 \left(E_{\alpha}^{(0)} + \sum_{j,\beta} W_{ij,\alpha\beta} d_{j,\beta} \right), \tag{5}$$

where $\mathbf{d}_i$ is the amplitude of the dipole moment induced on the ith particle, $\mathbf{E}^{(0)}$ is the applied field amplitude, and

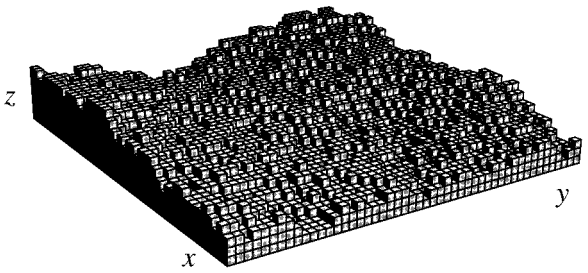

FIG. 1. The self-affine film obtained in the restricted solid-on-solid model. The scaling exponent $H = 0.4$ and the fractal dimension $D = 3 - H = 2.6$.

$$W_{ij,\alpha\beta} = -\frac{\delta_{\alpha\beta} r_{ij}^2 - 3\mathbf{r}_{ij,\alpha}\mathbf{r}_{ij,\beta}}{r_{ij}^5} \tag{6}$$

is the interaction operator between the two dipoles, with the radius vectors $\mathbf{r}_i$ and $\mathbf{r}_j$. The Greek indices denote the Cartesian tensor components (not to be confused with the polarizability, α).

Note that within the quasistatic approximation, a self-affine film can be thought of as a particle of very irregular shape. As shown in Refs. 12–14, the DDA is a good approximation for a particle of arbitrary material and shape provided the number of dipoles, N, is large enough that the boundary of the cubic array satisfactory approximates the desired particle (film, in our case) shape. A second necessary condition for the dipole array to provide an accurate representation of a homogeneous irregular object is that the length scale for variation of the field within the object must be large compared to the lattice period, a. For an object of a simple (e.g., convex) shape, the above criteria can be formulated quantitatively.[13] In our case, validity of the approximation can be checked out by performing numerical simulations for different N. The approximation is justified, if the obtained results do not vary with N (see below).

According to (2), there is a resonance at $\epsilon' = -2$. We introduce

$$X \equiv -Re[\alpha_0^{-1}] = -R_m^{-3} \left(1 + \frac{3(\epsilon' - 1)}{|\epsilon - 1|^2} \right)$$

and

$$\delta \equiv -\mathrm{Im}[\alpha_0^{-1}] = R_m^{-3} \frac{3\epsilon''}{|\epsilon - 1|^2},$$

where $\epsilon \equiv \epsilon' + i\epsilon''$. The variable X indicates a closeness to the resonance of an individual particle and, thus, plays the role of a frequency parameter, and δ characterizes dielectric losses. (The smaller δ the higher the quality factor, $q \sim \delta^{-1}$, of the resonance.) The general solutions to (5) and (6) expressed in terms of parameters X and δ depend only on morphology of an object; they are independent of material properties. Substituting a given dielectric function, $\epsilon = \epsilon(\lambda)$, to the above formulas, we can explicitly express parameters $X = X(\lambda)$ and $\delta = \delta(\lambda)$ in terms of the wavelength, i.e., the general solutions can be specified for any material.[16]

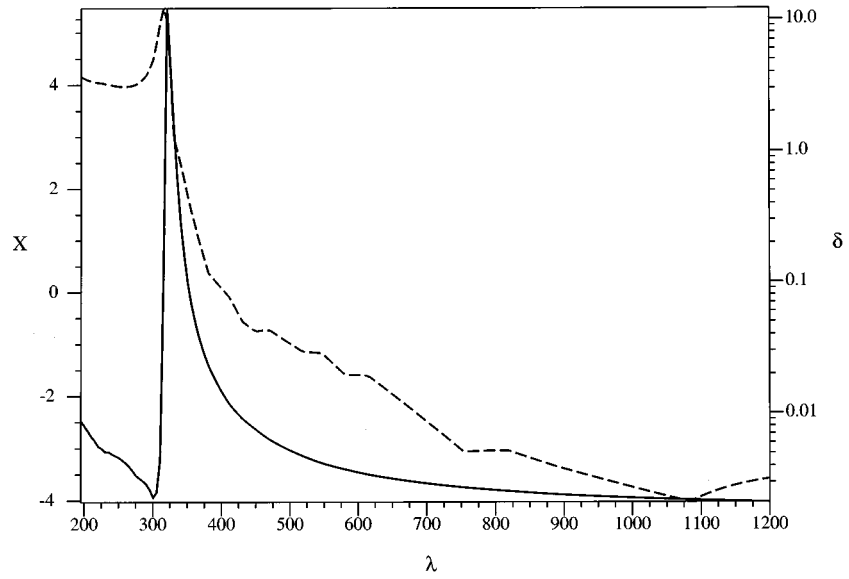

FIG. 2. The spectral variable, X (solid line), and decay parameter, δ (dashed line), versus the wavelength, λ, for silver particles in vacuum.

As an example, in Fig. 2, we show the wavelength dependences, $a^3X(\lambda)$ and $a^3\delta(\lambda)$, for silver particles (we used the data of Ref. 19 for $\epsilon(\lambda)$ in Ag). For X and δ near 350 nm and towards longer wavelengths, the λ dependences are associated with collective surface plasmon resonances. (Hereafter, we use units such that $a=1$.) As seen in Fig. 2, X changes significantly between 350 and 800 nm; hence, different dipole eigenmodes of a sample can be excited by applied fields with different frequencies. In the wavelength region from 800 nm toward longer wavelengths, $|\epsilon| \gg 1$ and X are almost constant [$X \approx X_0 = -a^3/R_m^3 = -4\pi/3$; see formulas (2) and (3)]. This means that a change in λ in this region does not change the resonant dipole mode, which can be referred to as the ''zero-frequency mode,'' or simply, as the ''zero mode.''[16] (Note, however, that, whereas $X \approx$ const for $\lambda > 800$ nm, the relaxation constant δ decreases for wavelength longer than 800 nm.)

As seen in Fig. 2, the allowed values of X for silver range approximately between -4 and 5; accordingly, on Ag film, only the modes with X values in this interval can be excited. These modes, however, cover a very broad spectral range including the ultraviolet, visible, and infrared regions of the electromagnetic spectrum.

To solve the CDE (5), we used a diagonalization of the interaction matrix (6). In terms of the eigenfunctions, $\psi_{n\alpha}(\mathbf{r}_i) \equiv (i\alpha|n)$, and eigenvalues, w_n, of the operator W, the solutions of the CDE (5) can be expressed as[16,20]

$$d_{i,\alpha} = \sum_{\beta} \alpha_{i,\alpha\beta} E_{\beta}^{(0)} = -\sum_{jn\beta} \frac{(i\alpha|n)(n|j\beta)}{(X+w_n)+i\delta} E_{\beta}^{(0)}. \qquad (7)$$

To perform calculations for large samples, with the number of particles (dipoles), N, forming a self-affine film more than 10 000, we used the Lanczos algorithm.[21]

In Fig. 3, we plot the density of the eigenmodes,

$$\rho(X) = \frac{1}{N} \left\langle \sum_n \delta(X - w_n) \right\rangle,$$

where the angular brackets denote averaging over an ensemble of samples. The mode density satisfies the following sum rule: $\int \rho(X)\,dX = 3$.[20] We used two different ensembles of random samples: one consisted of 12 relatively small samples, with $N \sim 10^3$, and the other one included four much larger samples, with $N \sim 10^4$ each. As seen in the figure, the results are close for the two ensembles. The modes cover a wide spectral interval, from $X \approx -5.3$ to $X \approx 9.5$. Note that for silver films, however, modes only in the range between -4 and 5 can be excited (see Fig. 2 and the following discussion).

In Figs. 4, we show plots for the real and imaginary parts of the ''parallel'' and ''perpendicular'' components of the mean polarizability per particle, $\alpha_{\parallel} \equiv (1/2)\langle \alpha_{i,xx} + \alpha_{i,yy} \rangle$ and $\alpha_{\perp} \equiv \langle \alpha_{i,zz} \rangle$. [The same, as in the case of $\rho(X)$, random ensembles were used for calculations of $\alpha(X)$.] The parallel component, $\alpha_{\parallel}$, characterizes the polarizability of a self-affine film in the (x,y) plane, whereas the perpendicular component, $\alpha_{\perp}$, gives the polarizability in the normal, z, direction. The polarizability components satisfy the sum rule: $\int \alpha_{\perp,\parallel}(X)\,dX = \pi$.[20]

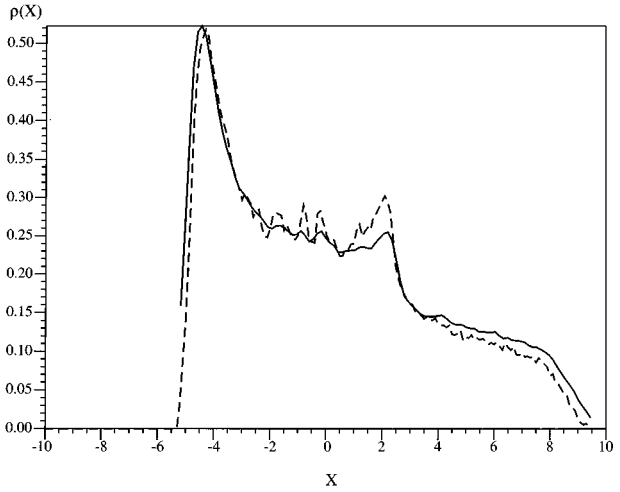

FIG. 3. Density of dipolar eigenmodes, $\rho(X)$, for the ensemble of self-affine samples consisting of $N \sim 10^3$ dipoles each (dashed line) and for the ensemble of larger samples, with $N \sim 10^4$ each (solid line).

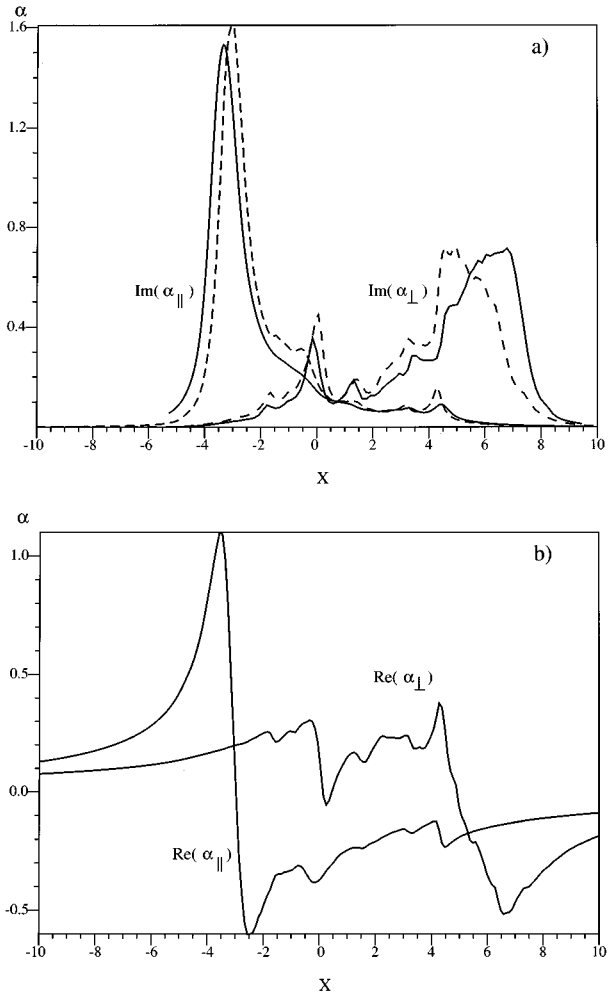

FIG. 4. The real (b) and imaginary (a) parts of the parallel, $\alpha_{\parallel}$, and perpendicular, $\alpha_{\perp}$, components of the polarizability. For Imα, the results for samples with $N\sim10^4$ and $N\sim10^3$ dipoles each (solid and dashed lines, respectively) are shown. For Reα, only the results of calculations with $N\sim10^3$ are shown (the results of calculations for Reα with $N\sim10^4$ are similar).

From the figures it is clear that there is a strong dichroism expressed in the difference between the two spectra, $\alpha_{\parallel}(X)$ and $\alpha_{\perp}(X)$. The modes contributing most to $\alpha_{\parallel}$ (the ''longitudinal'' modes) are located in the long wavelength part of the spectrum (negative X; see also Fig. 2), whereas the ''transverse'' modes tend to occupy the short wavelength part of the spectrum (positive X). To some extent, this can be understood by roughly considering a film as a prolate spheroid, where the longitudinal and transverse modes are shifted to the red and blue, respectively, in comparison with the eigenmode of a sphere. However, in contrast to the case of a spheroid, there is a large variety of eigenmodes in self-affine films, as follows from Figs. 3 and 4. Really, the widths of the spectra in Figs. 3 and 4 are much larger than the width of an individual resonance, δ; this indicates a strong inhomogeneous broadening associated with a variety of the dipolar eigenmodes on a self-affine surface. Thus, the dipole-dipole interactions of constituent monomers in a self-affine film ''generate'' a wide spectral range of resonant modes.

From Figs. 3 and 4, we also make an important conclusion that in the quasistatic approximation, the optical properties of a self-affine film do not depend on the number of monomers, N, and, therefore, on the linear size, l, of the film. The calculations that were performed for the ensembles of samples with very different numbers of particles and linear sizes give similar results. [We do not show in Fig. 4(b) the results of calculations for Re$\alpha(X)$ for the ensemble of samples with $N\sim10^4$; they are close to those obtained for the ensemble with $N\sim10^3$.] Note also that the fact that the spectra are almost independent of the number of the dipoles, N, justifies the used discrete dipole approximation.

The field distributions of eigenmodes on a self-affine surface are extremely inhomogeneous. On such surface, there are ''hot'' spots associated with areas of high local fields, and ''cold'' zones with small local fields. (Similar patchworklike picture of the field distribution is observed in fractal clusters.[16,22,23]) Spatial locations of the modes are very sensitive to both frequency and polarization of the applied field.

To demonstrate this, in Figs. 5, we show the intensity distributions for the local fields, $|\mathbf{E}(\mathbf{R}_i)|^2$, on the film-air interface [$E_{i,\alpha}\equiv E_{\alpha}(\mathbf{R}_i)=\alpha_0^{-1}d_{i,\alpha}$, where $d_{i,\alpha}$ are defined in (7), and $\mathbf{R}_i\equiv(x_i,y_i)$, where x_i and y_i are the coordinates of the dipoles on the surface of a film]. The results are shown for different values of frequency parameter, X, and polarizations of the applied field, $\mathbf{E}^{(0)}$. Note that the local field distributions, $|\mathbf{E}(\mathbf{R}_i)|^2$, can be measured with the use of a near-field scanning optical microscope, provided the probe is passive.[24]

As seen in Fig. 5, for a modest value of $\delta=0.03$, which is typical for metals in the visible and near-infrared parts of the spectrum, the local field intensities in the hot zones can significantly, up to three orders of magnitude, exceed the intensity of the applied field (for smaller values of δ, the enhancements can be even larger). The high frequency and polarization sensitivity of the field distributions is also obvious from the figure.

Strongly inhomogeneous distributions of local fields on a self-affine surface bring about large spatial fluctuations of local fields and strong enhancements of optical processes. These enhancements are especially large for nonlinear optical phenomena which are proportional to the local fields raised to some high power.

At first, we consider the field enhancements averaged over all particles (dipoles) forming a self-affine film, $\langle|\mathbf{E}_i|^2\rangle/|\mathbf{E}^{(0)}|^2$. By generalizing the result of Ref. 20 for nonsymmetric systems, such as rough thin films, we obtain that

$$G_{\parallel,\perp}=\delta\left(1+\frac{X^2}{\delta^2}\right)\mathrm{Im}\alpha_{\parallel,\perp}, \tag{8}$$

for the linearly polarized $\mathbf{E}^{(0)}$ that lies in the plane (x,y) and normal to it, respectively. According to (8), the enhancement factor $G\approx(X^2/\delta)\mathrm{Im}\alpha$ for $|X|\gg\delta$, i.e., it can be very large, provided Imα is not too small. Since a self-affine film is characterized by a strong inhomogeneous broadening, we anticipate large enhancements for this object [as seen in Figs. 3 and 4, Im$\alpha(X)$ is relatively large in a wide range of $|X|$, including the values $|X|\gg\delta$]. In the far Lorentz wing, when $|X|\to\infty$, the absorption Im$\alpha\approx\delta/X^2$ and $G\approx1$. For metals, however, X remains almost constant in the long-wavelength part of the spectrum, $|X|\approx|X_0|=-4\pi/3$ (see Fig. 2),

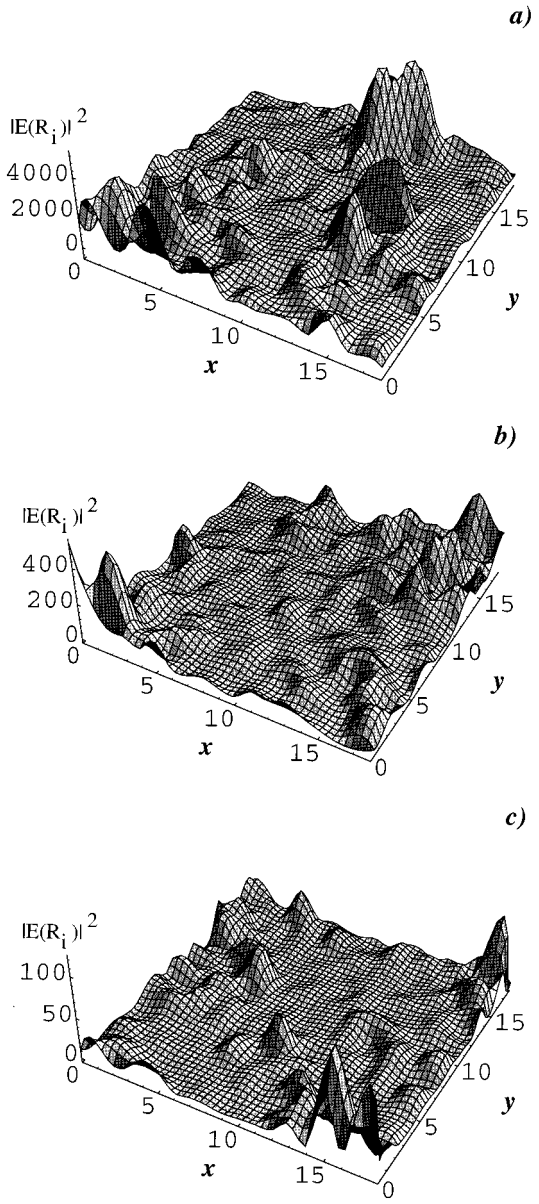

FIG. 5. Spatial distributions of the local field intensities, $|\mathbf{E}(\mathbf{R}_i)|^2$, on the self-affine surface for different values of frequency parameter, X, and polarizations of the applied field, $\mathbf{E}^{(0)}$. (a) $X=-3$, $\mathbf{E}^{(0)}=(2)^{-1/2}(1,1,0)$; (b) $X=-2$, $\mathbf{E}^{(0)}=(2)^{-1/2}(1,1,0)$; (c) $X=-3$, $\mathbf{E}^{(0)}=(0,0,1)$. The decay parameter $\delta=0.03$ in all the cases.

whereas δ decreases towards the longer wavelength ($\propto\lambda^{-1}$, according to the Drude model). Thus, in this region, $G\approx(X_0^2/\delta)\mathrm{Im}\alpha(X_0)\propto\lambda$, i.e., the enhancement increases towards the ir part of the spectrum.[16]

For thin films, it is more important to study the surface-averaged enhancement, with the averaging over particles on the interface only: $G_s\equiv\langle|\mathbf{E}(\mathbf{R}_i)|^2\rangle_s/|\mathbf{E}^{(0)}|^2$, where the sign $\langle\,\rangle_s$ denotes averaging over the dipoles on the surface of the film.

In Fig. 6(a), we show the results of our calculations for the enhancements, $G_{s\parallel}$ and $G_{s\perp}$, as functions of X, for the applied fields polarized along x and z, respectively. The decay parameter was set constant in these simulations, $\delta=0.03$. In Fig. 6(b), $G_{s\parallel}$ and $G_{s\perp}$ are plotted versus the

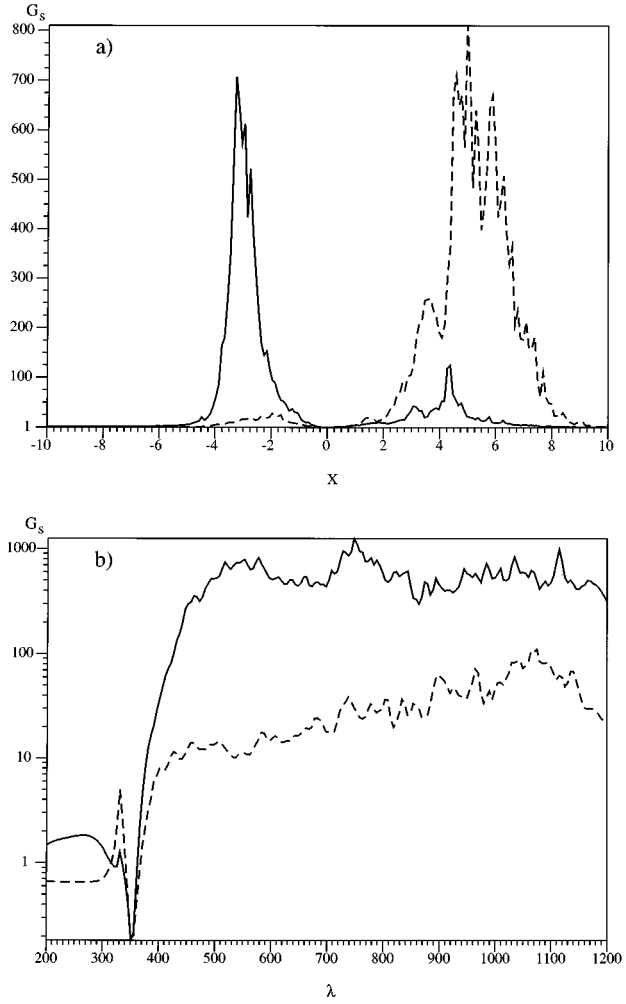

FIG. 6. The average enhancements, $G_{s\parallel}$ and $G_{s\perp}$, of local fields on the surfaces of self-affine films for the applied fields polarized along the x and z axes, respectively. (a) $G_{s\parallel}$ and $G_{s\perp}$ as functions of X ($\delta=0.03$); (b) $G_{s\parallel}$ and $G_{s\perp}$ as functions of λ for silver films. (The results are averaged over two samples).

wavelength, λ, for silver self-affine surfaces [the spectral dependencies, $X(\lambda)$ and $\delta(\lambda)$, were used; see Fig. 2]. As seen in Fig. 6(b), the enhancement, G_s, increases towards the long-wavelength part of the spectrum reaching the values $\sim 10^3$ for $G_{s\parallel}$. This is because the quality factors ($q\sim 1/\delta\sim|\epsilon-1|^2/3\epsilon''$) increase for the modes located in the long-wavelength part of the spectrum (see Fig. 2), that can easily be proved by using the Drude formula for the dielectric function $\epsilon(\lambda)$.[16] Thus, the dipole interactions shift the resonant frequencies toward the smaller frequencies where the quality factors for metals are significantly larger. (Therefore, the enhancements can be much larger than for an isolated metal sphere; to some extent, similar effects occur for the longitudinal mode in a prolate spheroid.[2])

To study localization of eigenmodes on a self-affine surface, we calculated the mode pair-correlation function defined as

$$\nu_n(R)=\frac{1}{C}\sum_{i\alpha}[(i\alpha|n)]^2\times\left(\frac{1}{\pi(2R\rho+\rho^2)}\sum_{j,\beta;R\leqslant R_{ij}<R+\rho}[(j\beta|n)]^2\right), \tag{9}$$

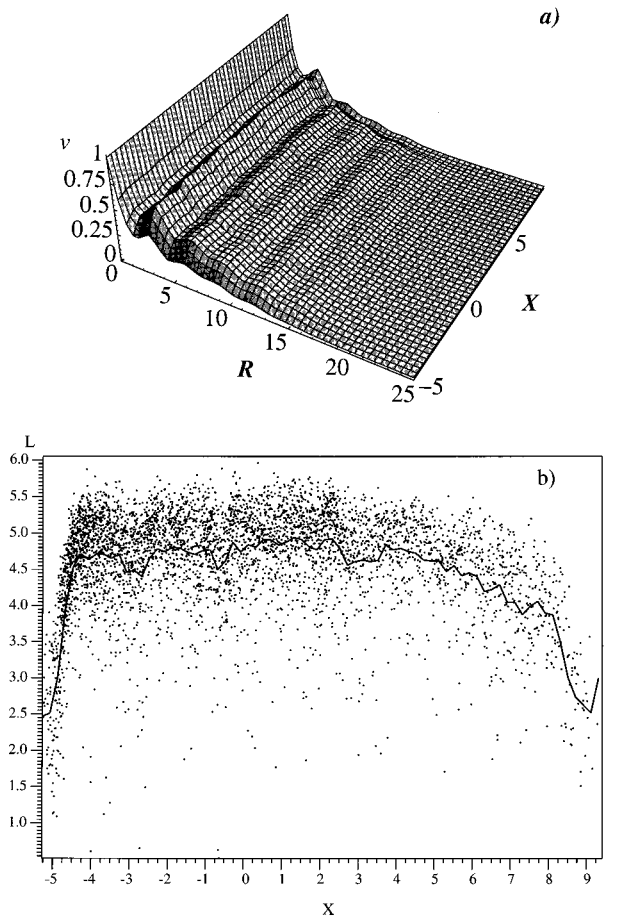

FIG. 7. (a) The mode correlation function, $\nu(R,X)$. (b) The mode correlation length, L_n (dots), and the average correlation length, $L(X)$ (solid line). (The averaging was performed for the spectral interval $\Delta X=0.2$ for 2 random samples; see the text for details).

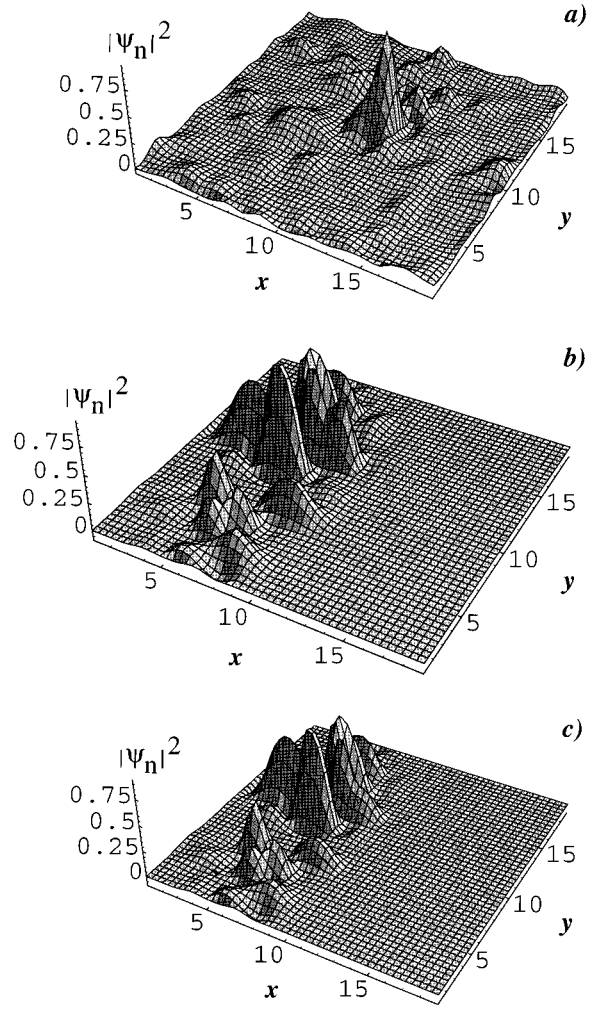

FIG. 8. The spatial distribution, $|\psi_n|^2=\Sigma_\alpha|(i\alpha|n)|^2$, for the mode with the eigennumber $w_n\approx 0.16$ (a). The distribution, $\Sigma_\alpha|(i\alpha|n)|^2$, for the mode with the minimum eigennumber, $w_n\approx -5.25$, for an original sample (b), and for the sample obtained from the original one by removal the whole part of the film with coordinates $x\geqslant 10$. (Arbitrary units are used for the vertical axis).

where the normalization constant C is defined by the requirement $\nu(0)=1$, and the summations are over dipoles on the surface only. The sum over j in Eq. (9) includes the dipoles within the ring formed by the circles (around the ith dipole) of radii R and $R+\rho$; the area of the ring is $\pi(2R\rho+\rho^2)$, and ρ is small, $\rho=1.5a$, in our calculations. [Note that definition (9) can be formally written as

$$\nu_n(R)\sim\Sigma_{i,j\in s;\alpha,\beta}\delta(R_{ij}-R)[(i\alpha|n)]^2[(j\beta|n)]^2,$$

where $\mathbf{R}_{ij}\equiv\mathbf{R}_i-\mathbf{R}_j$.[25]] If the mode is localized within a certain area of radius R_0, then $\nu(R)$ is small for $R>R_0$ and the rate of decay of $\nu(R)$ at $R>R_0$ reflects a character of localization (strong or weak) for the state n.[27]

The formula (9) is a discrete function of its argument, n. To obtain a smooth correlation function, $\nu(R,X)$, we average $\nu_n(R)$ over small interval ΔX for an ensemble of random samples:

$$\nu(R,X)=\left\langle [K(X,\Delta X)]^{-1}\sum\ \nu_n(R)\right\rangle, \qquad (10)$$

where the summation is taken over all n such that $|X-w_n|\leqslant\Delta X$ and $K(X,\Delta X)$ is the number of terms in the sum.

The results of our calculations of $\nu(R,X)$ averaged over two samples are shown in Fig. 7(a). The linear size of both square samples is $l=19$ so that the largest value of R is $\sqrt{2}l\approx 27$.

The calculated $\nu(R,X)$ are well approximated by the formula $\nu(R,X)=\exp\{-[R/L(X)]^\kappa\}$, where $\kappa\approx 0.7$ (rms for the used approximation was about 7×10^{-2}). When the exponent is larger than one, $\kappa>1$, the modes are commonly called superlocalized; in our case, with $\kappa\approx 0.7$, the modes can be referred to as sublocalized (or quasilocalized), on average.

Note that for individual modes, the best fit of $\nu_n(R)$ in (9) can be achieved with varying κ_n; then, the values of κ_n range from 0.4 to 1.1. This indicates that there are, in general, both kind of modes: superlocalized ($\kappa_n>1$) and sublocalized ($\kappa_n<1$). However, after averaging over small ΔX for an ensemble of random samples, the dependence $\nu(R,X)$ in (10) is well approximated by the function $\exp\{-[R/L(X)]^\kappa\}$ with constant $\kappa\approx 0.7$. Thus, although the

degree of localization is different for different modes, we can say that, on average, the modes are sublocalized.

In Fig. 7(b), we plot random correlation lengths, L_n, for individual modes, where L_n (dots in the figure) are found from the formula $\nu_n(R)=\exp[-R/L_n]^{\kappa}$, when it is used to interpolate the results of calculations of $\nu_n(R)$ in (9). [For the sake of simplicity, L_n shown in Fig. 7(b) were found assuming that $\kappa_n=\kappa=0.7$ for all modes; the results of calculations for L_n with adjustable κ_n are qualitatively similar.] The solid line in Fig. 7(b) represents the average correlation length, $L(X)$, found from the relation $\nu(R,X)=\exp[-R/L(X)]^{\kappa}$ ($\kappa=0.7$), that was applied to interpolate $\nu(R,X)$ in (10). As seen in the figure, $L(X)\approx 4.5$ for most of the eigenmodes, and it decreases down to $L(X)\approx 2$ for the modes close to the edges of the spectrum.

To illustrate localization of modes, in Fig. 8(a), we plot $|\psi_n|^2=\Sigma_{\alpha}[(i\alpha|n)]^2$ for the mode with $w_n\approx 0.16$ as a function of the position on the surface, $\mathbf{R}_i$ (arbitrary units are used for the vertical axis). In Fig. 8(b), we also show the mode with the minimum eigennumber, $w_n\approx -5.25$. This mode is localized in only one, x, direction. It is interesting to note that removal of the whole part of the sample with $x\geqslant 10$ almost does not change the mode distribution [Fig. 8(c)].

We also calculated optical properties for random films obtained from the original self-affine films by their partial smoothing. As was mentioned, a self-affine surface simulates a thin film deposited on a cold substrate. Heating up the substrate allows a deposited particle to diffuse on the surface searching for an energetically more stable position; this results in a partial smoothing of the film. To simulate approximately the heating (annealing) of a self-affine film, each particle which initially had less than three neighbors (bonds) was moved to the nearest position where the particle had three or more bonds. As a next step, we allowed particles to move to near positions, provided this results in decreasing the average height of the film; then, the film was again smoothed by the first procedure. To some extent, the described processes simulate film annealing and can be used to model surfaces which are smoother than the original self-affine surfaces, but still random.

We briefly mention the main results obtained in our calculations for the smoothed films (the corresponding figures are not shown). The smoothing of films results in a decreased inhomogeneous broadening; in accordance with this, the spectral range where enhancements occur is also decreased. (We note, however, that the absolute maximum for the enhancement on smoothed films can be larger than that on self-affine films.) For metal smoothed films, in the important long-wavelength part of the spectrum, the enhancement is less than for the original self-affine surfaces (by about an order of magnitude). The modes on the smoothed films also show some tendency to localization (similar to the case of self-affine surfaces, they are quasilocalized).

To summarize, we showed that for a self-affine surface the spatial distributions of local fields are extremely inhomogeneous and consist of hot and cold zones. Some of the dipolar eigenmodes on a self-affine film are strongly localized (whereas others involve into excitation a significant fraction of the film). The local field distributions are very sensitive to the frequency and polarization of the applied field. Large spatial fluctuations of local fields bring about strong enhancements of optical processes on a self-affine film.

We also note that the results reported here are valid within the quasistatic approximation, i.e., they can be applied only to films with the lateral size smaller than the wavelength. Though the optical properties of self-affine films with the size larger than the wavelength are probably, in many respects, similar to those considered here, there are significant differences anticipated as well.

Work at NMSU was supported in part by NSF under Grant No. DMR-9500258 and by NATO under Grant No. CRG 950097; work at Université Paris-Sud was supported by NATO under Grant No. CRG 950097; work at Sandia National Laboratories was supported by the U.S. Department of Energy under Contract No. DE-AC04-94AL85000. One of us (V.S.) is grateful to V. Markel for useful comments and to The Association of Western Universities, Inc. for support of his work at Sandia National Laboratories (Albuquerque, NM) during the summer of 1995.

[1] R. Chiarello, V. Panella, J. Krim, and C. Thompson, Phys. Rev. Lett. **67**, 3408 (1991); J. Krim, I. Heyvaert, C. Van Haesendonck, and Y. Bruynseraede, *ibid.* **70**, 57 (1993).

[2] *Surface Enhanced Raman Scattering*, edited by R. K. Chang and T. E. Furtak (Plenum Press, New York, 1982).

[3] C. Douketis, Z. Wang, T. L. Haslett, and M. Moskovits, Phys. Rev. B **51**, 11 022 (1995).

[4] M. Kardar, G. Parisi, and Y. C. Zhang, Phys. Rev. Lett. **56**, 889 (1986).

[5] *Dynamics of Fractal Surfaces*, edited by F. Family and T. Vicsek (World Scientific, Singapore, 1991).

[6] The complete set of formulas for the case of electromagnetic waves scattering from smooth random surfaces can be found, e.g., in Refs. 7 and 8.

[7] A. Marvin, T. Toigo, and V. Celli, Phys. Rev. B **11**, 2777 (1975); F. Toigo, A. Marvin, V. Celli, and N. Hill, *ibid.* **15**, 5618 (1977).

[8] A. A. Maradudin and D. L. Mills, Phys. Rev. B **11**, 1392 (1975).

[9] P. Beckmann and A. Spizzichino, *The Scattering of Electromagnetic Waves from Rough Surfaces* (Artech, Norwood, Mass., 1987).

[10] A. Ishimaru, in *Scattering in Volumes and Surfaces*, edited by M. Nieto-Vesperinas and J. C. Dainity (Elsevier Science Publishers, New York, 1990).

[11] R. M. Fitzgerland and A. A. Maradudin, Waves in Random Media **4**, 275 (1994).

[12] E. M. Purcell, C. R. Pennypacker, Astrophys. J. **186**, 705 (1973).

[13] B. T. Draine, Astrophys. J. **333**, 848 (1988).

[14] A. Lakhtakia, Optik **91**, 134 (1992).

[15] S. B. Singham and C. F. Bohren, J. Opt. Soc. Am A **5**, 1867 (1988).

[16] Vladimir M. Shalaev, Phys. Rep. **272**, 61 (1996); V. A. Markel, Vladimir M. Shalaev, E. B. Stechel, W. Kim, and R. L. Arm-

strong, Phys. Rev. B **53**, 2425 (1996); Vladimir M. Shalaev, E. Y. Poliakov, and V. A. Markel, *ibid.* **53**, 2437 (1996).
[17] P. Meakin, P. Ramanlal, L. M. Sander, and R. C. Ball, Phys. Rev. A **34**, 5091 (1986).
[18] J. M. Kim and J. M. Kosterlitz, Phys. Rev. Lett. **62**, 2289 (1989).
[19] P. B. Johnson and R. W. Christy, Phys. Rev. B **6**, 4370 (1972).
[20] V. A. Markel, L. S. Muratov, M. I. Stockman, and T. F. George, Phys. Rev. B **43**, 8183 (1991).
[21] J. K. Collum and R. A. Willoughby, *Lanczos Algorithm for Large Symmetric Eigenvalue Computations* (Burkhauser, Boston, 1985), Vol. 1; *Solid State Physics* (Academic Press, New York, 1980), Vol. 35.
[22] V. M. Shalaev, R. Botet, and A. V. Butenko, Phys. Rev. B **48**, 6662 (1993).
[23] D. P. Tsai, J. Kovacs, Z. Wang, M. Moskovits, V. M. Shalaev, J. Suh, and R. Botet, Phys. Rev. Lett. **72**, 4149 (1994); Vladimir M. Shalaev and Martin Moskovits, *ibid.* **75**, 2451 (1995).
[24] E. Betzig *et al.*, Science **257**, 189 (1992).
[25] Recently we learned that similar correlation function was introduced in Ref. 26, for description of eigenmodes in fractals.
[26] M. I. Stockman, L. N. Pandey, and T. F. George, Phys. Rev. B **53**, 2183 (1996).
[27] A. Petri and L. Pietronero, Phys. Rev. B **45**, 12 864 (1992).